Catalysis
Science & Technology

Accepted Manuscript

This is an *Accepted Manuscript*, which has been through the RSC Publishing peer review process and has been accepted for publication.

Accepted Manuscripts are published online shortly after acceptance, which is prior to technical editing, formatting and proof reading. This free service from RSC Publishing allows authors to make their results available to the community, in citable form, before publication of the edited article. This *Accepted Manuscript* will be replaced by the edited and formatted *Advance Article* as soon as this is available.

To cite this manuscript please use its permanent Digital Object Identifier (DOI®), which is identical for all formats of publication.

More information about *Accepted Manuscripts* can be found in the **Information for Authors**.

Please note that technical editing may introduce minor changes to the text and/or graphics contained in the manuscript submitted by the author(s) which may alter content, and that the standard **Terms & Conditions** and the **ethical guidelines** that apply to the journal are still applicable. In no event shall the RSC be held responsible for any errors or omissions in these *Accepted Manuscript* manuscripts or any consequences arising from the use of any information contained in them.

Dimerization of ethene in a fluidized bed reactor using Ni-based Supported Ionic Liquid Phase (SILP) catalysts

Florian T. U. Kohler [a], Konstantin Gärtner [a], Veit Hager [a], Marco Haumann [a]*, Michelle Sternberg [b], Xinjiao Wang [b], Normen Szesni [c], Karsten Meyer [b], Peter Wasserscheid [a]*

[a] *Department of Chemical and Bioengineering, Reaction Engineering, University Erlangen-Nuremberg, Egerlandstraße 3, D-91058 Erlangen, Germany; e-mail: marco.haumann@fau.de, peter.wasserscheid@crt.cbi.uni-erlangen.de*
[b] *Department of Chemistry and Pharmacy, Inorganic Chemistry, University Erlangen-Nuremberg, Egerlandstraße 1, D-91058 Erlangen, Germany*
[c] *Clariant Produkte (Deutschland) GmbH, Waldheimer Straße 13, D-83052 Bruckmühl, Germany*

Abstract

The complexes [(mall)Ni(dppanis)][SbF$_6$] (mall = methallyl, dppanis = (2-methoxyphenyl)diphenylphosphine) **1**, [(mall)Ni(PPh$_3$OC$_{10}$)][SbF$_6$] (PPh$_3$OC$_{10}$ = (2-decyloxyphenyl)diphenylphosphine) **2**, and [(mall)Ni(PPh$_3$OdiMePh)][SbF$_6$] (PPh$_3$OdiMePh = (2-(2,6-dimethylphenoxy)phenyl)diphenylphosphine) **3** were immobilized as Supported Ionic Liquid Phase (SILP) catalysts and applied for the tandem dimerization/isomerization of ethylene to 2-butene in a fluidized bed reactor. The better heat removal in the fluidized bed improves the catalyst stability and allows for a more detailed investigation of the deactivation mechanism. Based on kinetic studies, a second order deactivation mechanism is proposed, in which two nickel complexes dimerize if supply of ethene is insufficient.

Introduction

Over the last decades, on-purpose routes for the production of propene from ethene (ethene to propene, ETP) have attracted increasing interest due to a shifting demand from polyethylene to polypropylene.[1-3] The ETP sequence involves dimerization of ethene to 1-butene and consecutive isomerization to 2-butene. Metathesis of the formed 2-butene with ethene finally yields propene. Literature known systems for these consecutive reactions include heterogeneous catalysts, such as e. g. zeolites, supported molybdenum, tungsten oxide, tungsten hydride or nickel ions loaded on MCM-41.[4-11] We recently reported an immobilized version of cationic, homogeneous nickel complexes that allow the dimerization and isomerization of ethylene to 2-butene with an exceptionally high selectivity.[12] Such nickel complexes were tested in the past for ethylene oligomerization to alpha-olefins but were discarded due to their disadvantageous high isomerization activity.[13] Homogeneous nickel complexes are well known oligomerization catalysts following a nickel-hydride chain growth mechanism in which the competition between chain growth and termination via β-hydride elimination is governing the product distribution.[14-16] While neutral nickel complexes usually produce higher alkenes in a relative wide Schulz-Flory distribution, short alkenes are mainly obtained with cationic catalysts.[17,18] Amongst those, methallyl nickel complexes, predominantly with phosphinocarboxylates as ligands, displayed high oligomerization and isomerization activities already at mild temperatures and at low ethylene pressures (see Figure 1 for the complexes [(mall)Ni(dppanis)][SbF$_6$] (dppanis = (2-methoxyphenyl)diphenylphosphine) **1**, [(mall)Ni(PPh$_3$OC$_{10}$)][SbF$_6$] (PPh$_3$OC$_{10}$ = (2-decyloxyphenyl)diphenylphosphine) **2**, and

[(mall)Ni(PPh₃OdiMePh)][SbF₆] (PPh₃OdiMePh = (2-(2,6-
dimethylphenoxy)phenyl)diphenylphosphine) **3**).[19-26]
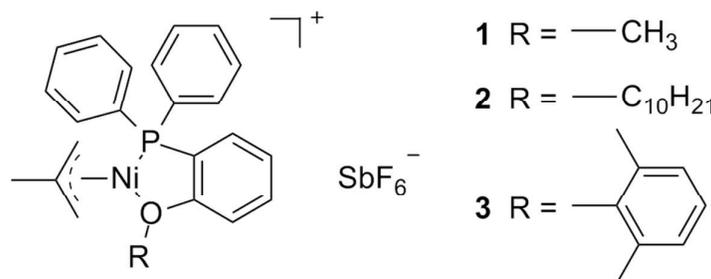
Figure 1. *Cationic nickel catalyst complexes applied for the tandem dimerization/isomerization of ethene to 2-butene.*

Due to their ionic nature, these nickel complexes can be dissolved in ionic liquids.[27-30] By dispersing the so-obtained ionic catalyst solutions on a highly porous inorganic support, solid materials are obtained that can be handled like classical heterogeneous catalysts.[31,32] These supported ionic liquid phase (SILP) catalysts, depicted in Figure 2, have been applied in a variety of reactions, both in liquid and gas phase contact.[33] Due to the extremely low volatility of ionic liquids, the SILP concept is ideally suited for continuous gas-phase processes.[34]
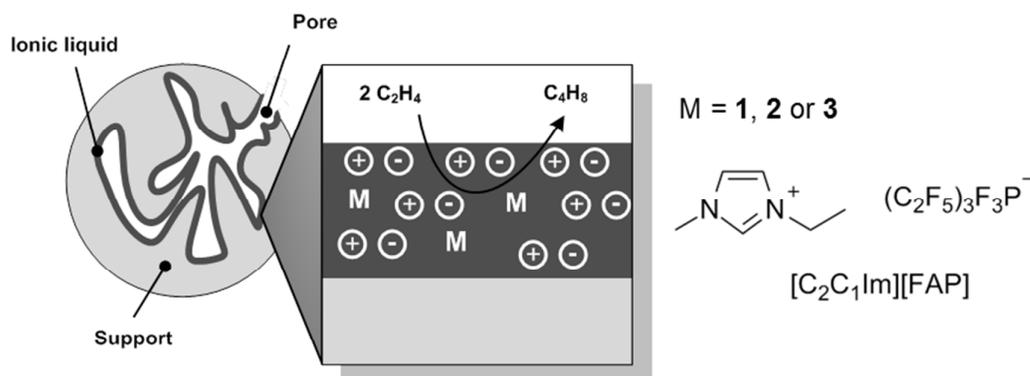
Figure 2. *Schematic representation of the applied Ni-based SILP catalyst systems.*

For the gas-phase dimerization/isomerization of ethene in the presence of the cationic Ni-SILP catalysts **1** to **3**, the complexes were dissolved in the ionic liquid [C₂C₁Im][FAP] (see Figure 2) and dispersed as thin film over silica gel 100 support.[12] These SILP catalysts showed high activity in the first phase of the reaction, exemplified by an initial turn-over frequency TOF_0 of around 520 mol_{butene} mol_{Ni}^{-1} h^{-1}. Catalyst stabilities were reasonable and reached overall turn-over numbers (TONs) ranging from 53,300 (for complex **1**) to 97,700 (for complex **3**) at 19 °C. The low reaction temperature was required to avoid thermal decomposition of the cationic Ni-complexes.[35] Under these conditions, the combination of high catalytic activity and strong exothermicity of the dimerization reaction still resulted in hot spot formation inside the fixed catalyst bed. The temperature at the top end of the fixed bed (T_{top}) and the temperature at the bottom end of the fixed bed (T_{bottom}) were measured over time by two thermocouples (Figure 3). At the beginning of the reaction, a severe rise in temperature to $T_{top} =$ 59 °C was observed, while the temperature at the bottom end increased to only 42 °C. After that, the

temperature at the top rapidly decreased approximating the cooling temperature T_c while the temperature at the bottom end slowly increased. With concomitant approach of the maximum temperature at the bottom of $T_{bottom} = 56\ °C$, a drop in conversion occurred. The observed course of temperature indicates deactivation of the catalyst by a migrating reaction/deactivation front as schematically depicted in Figure 6. This front obviously first develops at the top end of the fixed bed reactor where ethene contacts the catalyst bed. Due to the high activity of the applied cationic nickel complexes, full conversion of ethene occurs in this upmost layer of the fixed bed. Accordingly, the major part of the reaction heat ($\Delta H_R = -112.3\ kJ\ mol^{-1}$) is released in this layer and a temperature hot spot forms resulting in the thermal deactivation of the dissolved Ni-complex.

SILP catalyst particle: ○ non-activated ● catalytically active ○ thermally decomposed
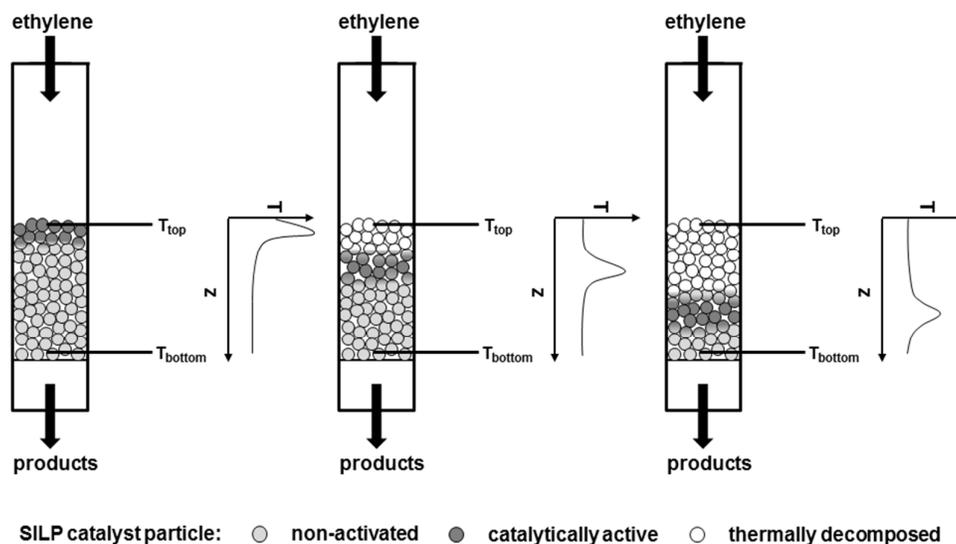
Figure 3. Schematic representation of the reaction/deactivation front moving through the fixed bed containing the SILP catalyst.

Once a certain layer of the catalyst bed has been deactivated the reaction front moves to the next layer; again, inducing a rise in temperature followed by thermal catalyst deactivation. In this manner, a reaction/deactivation front migrates through the entire fixed bed until it reaches the bottom and the whole system turns inactive.

Remarkably, these hot spot formation problems could neither be improved by diluting the SILP catalyst with inert material nor by lowering the nickel content nor by increasing the content of inert gas in the reaction mixture. Note that the failure of all these well-established ways to circumvent hot spots in fixed bed reactors is linked to the extreme sensitivity of cationic Ni-complexes against humidity and all traces of nucleophiles that may act as strong catalyst poisons.

In the present work we report on the application of fluidized bed reactor technology to improve the heat removal from the SILP catalyst. It is anticipated that increased isothermicity in the reactor will lead to prolonged catalyst stability. To the best of our knowledge, the here described work represents the first attempt to apply SILP catalysts in a fluidized bed reactor.

Results and discussion

Fluidization behavior of silica based support materials

We first conducted a detailed characterization of appropriate SiO_2-based porous support materials and their fluidization behavior in a nitrogen carrier flow. An overview of the tested support material and their characteristics is given in Table 1. The measured particle size distribution, bulk density, and minimum fluidization velocities of the support materials applied in a fluidized bed reactor are listed as well.

Table 1. Characteristics of SiO_2-based porous support materials and their minimum fluidization velocity v_{mf} for the fluidization in a nitrogen flow.

Entry	Support	V_{pore} [a]	S_{BET} [b]	d_{pore} [c]	δ [d]	x_{50} [e]	$v_{mf,meas}$ [f]	$v_{mf,calc}$ [g]
		ml g^{-1}	m^2 g^{-1}	nm	g cm^{-3}	μm	cm s^{-1}	cm s^{-1}
1	**S1** [h]	0.455	111.9	13.9	3.203	68.5	0.25	0.18
2	**S2** [h]	0.578	216.6	17.3	2.525	58.7	0.11	0.09
3	**S3** [h]	0.958	182.3	12.6	2.356	98.8	0.21	0.28
4	**S4** [h]	0.732	191.4	9.1	2.664	89.0	0.35	0.26
5	**S5** [h]	0.732	296.2	7.0	2.129	56.0	0.16	0.08
6	**S6** [h]	0.784	229.5	8.8	2.104	57.0	0.17	0.08
7	**S7** [h]	0.972	346.2	11.0	2.650	123.8	0.37	0.57
8	**S8** [i]	0.483	180.3	4.7	1.921	120.9	n.d.	0.34
9	**S9** [j]	1.392 [k]	45.7 [k]	130 [k]	2.218	80.7	0.11	0.18
10	**S10** [j]	1.381 [k]	54.4 [k]	57.7 [k]	2.489	95.1	0.22	0.24
11	**S11** [j]	1.392 [k]	45.7 [k]	130 [k]	2.218	47.8	0.10	0.06
12	**S12** [i]	0.855	346.5	7.0	2.070	59.5	0.17	0.09

a) Pore volume; b) surface area according to BET method; c) average pore diameter; d) density; e) mean particle size; f) minimum fluidization velocity, measured; g) minimum fluidization velocity, calculated according to [36] as summarized in [37]; h) supplied by Clariant; i) supplied by Merck KgaA; j) supplied by VitraBio; k) manufacturer's data by means of mercury intrusion method.

In 1973, Geldart classified four different groups of solids applied in gas-solid fluidized beds regarding their fluidization behavior [38]. Group A solids are aeratable and form a homogenous fluidized bed, whereas Group B particles lead to rising gas bubbles inside the fluidized bed. Group C particles are very small and cohesive and thus a fluidization is hardly realizable. Particles related to group D are relative huge and fluidized beds tend to build a spouted bed with gas channels. From the Geldart classification of our support materials shown in Figure 4a) it became obvious that some supports (**S2**, **S5**, **S6** and **S12**) can be classified as part of Geldart group A, while most SiO_2-based porous supports are in the boundary region between Geldart group A and B (**S1**, **S3**, **S4**, **S8**, **S10** and **S11**). Only **S7** can clearly be assigned to Geldart B; most likely forming a bubbling fluidized bed. These results were confirmed by the pressure drop curves of the investigated materials given in the ESI. The minimum fluidization velocity $v_{mf,meas}$ determined for these materials indicated also the best fluidization performance for the support **S5** and **S11** (entries 5 and 11). The measured values are in the range of the predicted minimum fluidization velocity $v_{mf,calc}$ calculated according to literature procedure [36,37] (for equation see supporting information).
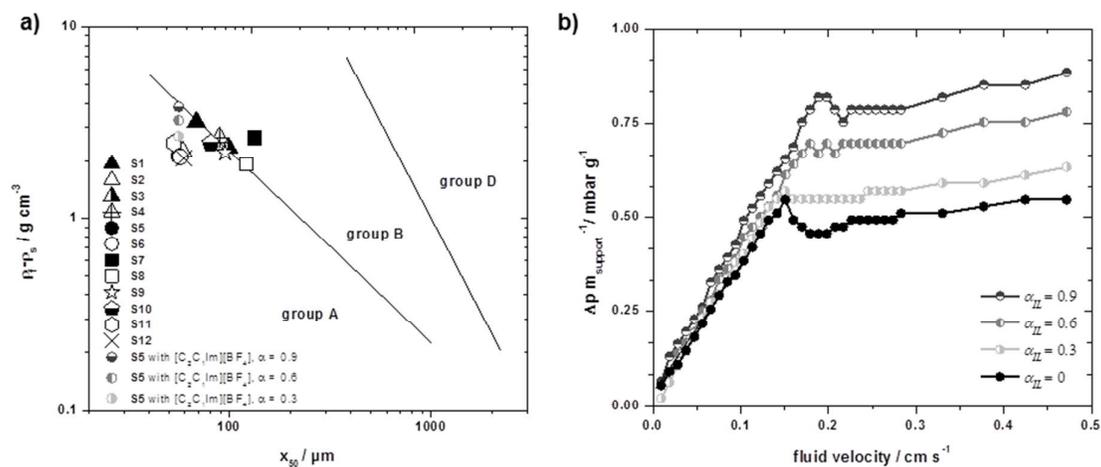
Figure 4. *a) Classification of porous support materials according to Geldart; mean particle size from particle size distribution and solid density. b) Specific pressure drop curves of the support* ***S5*** *(α_{IL} = 0) and SILP-systems consisting of* ***S5*** *with different pore filling of $[C_2C_1Im][BF_4]$ (α_{IL} = 0.3, 0.6 and 0.9); m_{bed} = 5 g, d_i = 16 mm, $V_{nitrogen}$ = 2-100 ml min^{-1}.*

In a consecutive fluidization experiment we were interested in the change of the fluidization characteristics of SILP-systems compared to the respective neat support material. We therefore prepared SILP-particles based on **S5** with different amounts of the ionic liquid 1-ethyl-3-methylimididazolium tetrafluoroborate ($[C_2C_1Im][BF_4]$). The measured pressure drop curves of **S5** and the SILP-systems based on **S5** with a pore filling degree of α_{IL} = 0.3, 0.6 and 0.9 are shown in Fig. 4b). The results indicate that with a higher ionic liquid loading both the overall pressure drop and the minimum fluidization velocity (v_{mf} from 0.15 cm s^{-1} for α_{IL} = 0 to 0.20 cm s^{-1} for α_{IL} = 0.9) are increasing. A homogenous fluidization, however, is still possible using **S5** with an ionic liquid pore filling of α_{IL} = 0.9 of $[C_2C_1Im][BF_4]$. Obviously the Geldart classification specifies these SILP-systems to behave still like Geldart A particles.

In a preliminary catalytic experiment we investigated the performance of the SILP catalyst (**S5**, $[C_2C_1Im][FAP]$, α_{IL} = 0.3, Ni-loading = 0.25 wt.-%) in a fluidized bed reactor using an undiluted ethene flow as feedstock at a flow rate of 25.5 Nml min^{-1}. An incomplete fluidization of the fluidized SILP bed was observed, caused by the decrease of the volume flow due to the volume contraction during the dimerization reaction. Additionally, the condensation of high-boiling by-products, mainly hexenes and octenes, in the porous SILP material turned out to be a severe drawback; and consequently, the SILP particles agglomerated in the course of the experiment. Increasing the volume flow of ethene to 51 Nml min^{-1} gave also an undesirable result, as the temperature inside the catalyst bed instantaneously rose to around 353 K. This could be attributed to the high exothermicity of the dimerization reaction and led to an immediate deactivation of the temperature sensitive Ni catalyst. In consecutive experiments we therefore diluted the ethylene feed with argon in order to sustain the fluidization of the SILP catalyst bed. Under these conditions, no temperature increase was detectable while the fluidization of the catalyst bed was conserved. Details of these preliminary experiments are given in the Supporting Information.

Comparison of fixed bed and fluidized bed dimerization

The dimerization of two diluted ethene substrate flows, purified and non-purified (for details see Experimental Part), in both fixed bed und fluidized bed operation of the reactor was investigated and Table 2 compiles the parameter of the SILP catalysts, the reaction conditions, and the catalytic results

(Entries 14-17). Figure 5a) represents the comparison of both operation modes by showing the conversion and selectivity over time-one-stream (TOS).
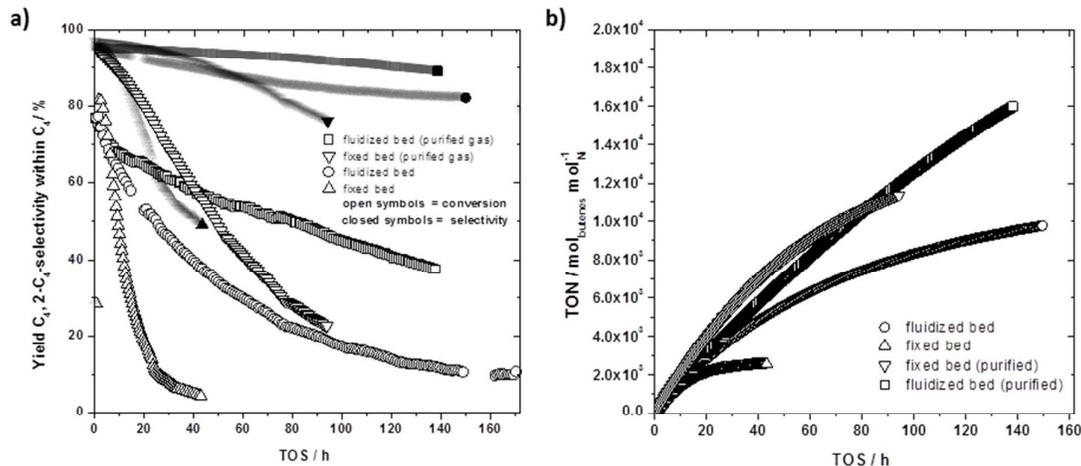
Figure 5. *Comparison of conversion, selectivity of 2-butenes within C$_4$-fraction and TON of fixed and fluidized bed dimerization of purified and non-purified diluted ethene stream with the SILP catalyst [(mall)Ni-dppanis][SbF$_6$]* ***1****, w$_{Ni}$ = 2.50 mg$_{Ni}$ g$_{support}$$^{-1}$,* ***S5****, [C$_2C_1$Im][FAP], α$_{IL}$ = 0.3; m$_{SILP}$ = 1000 mg, T$_{reactor}$ = 292 K, p$_{ethene}$ = 68 mbar, V$_{ethene}$ = 5.1 Nml min^{-1}, τ ≈ 1.3 s, p$_{reaction}$ = 1 bar.*

The results for both feeds (purified and non-purified ethene and argon) show a significant difference between the fixed bed and fluidized bed operation, as expected. The fixed bed experiment with non-purified feeds (Entry 14, Table 2) showed a constant conversion level of above 80 % for 3 h, followed by a pronounced decrease of conversion within the next 20 h. This deactivation was accompanied by a distinct decrease of the 2-butene selectivity, which dropped from 95 % to 75 % at the residual conversion of 20 %. The turn-over number at 50 % activity TON$_{t1/2}$ was 1.55 10^3 mol$_{butene}$ mol$_{Ni}$$^{-1}$. In contrast, the fluidized bed experiment (Entry 15) showed an instantaneous decrease of the conversion of ethene, but also a prolonged deactivation time to reach a residual conversion of 20 % at which the 2-butene selectivity was still 85 %. The TON$_{t1/2}$ was almost 2.8 times higher than for the comparable fixed bed experiment. This indicates an improved distribution of the released reaction heat throughout the fluidized catalytic bed. Within the fixed bed experiment hot spots are formed, resulting in a faster deactivation due to the temperature sensitivity of the Ni catalyst.

The two reactor types also gave different results when using purified (ethene and argon with H$_2$O and O$_2$ ≤ 15 ppb) instead of standard feed with the latter yielding lower stability. In the fixed bed (Entry 16, Table 2) the catalyst showed a higher initial activity compared to standard feed and the long-term stability of the fluidized bed experiment (Entry 17, Table 2) was higher. The turn-over number (TON) over time-on-stream TOS, shown in Figure 5b) demonstrates the improved stability of the SILP catalysts used in a fluidized bed reactor, as these TON values exceed the TON of the corresponding fixed bed experiment by almost a factor of two. Moreover, the better stability with purified gas suggests at least one additional deactivation mechanism besides the thermal decomposition. This deactivation mechanism obviously involves impurities in the feed streams, such as traces of oxygen or moisture.

Table 2. SILP catalyst composition, reaction conditions and results from fluidized bed dimerization experiments.

Entry	Support	ω_{Ni} [a]	m_{SILP} [b]	$T_{reactor}$	p_{ethene}	TOF_{max} $mol_{butene}\,mol_{Ni}^{-1}$	$t_{1/2}$ [c]	$TON_{1/2}$
		wt‰	g	K	10^{-3} bar	h^{-1}	h	$mol_{butene}\,mol_{Ni}^{-1}$
13	**S5**	2.50 [d]	1	292	68	181	10.9	1550
14	**S5**	2.50 [e]	1	292	68	189	34.2	4280
15	**S5**	2.50 [g]	1	292	68	215	49.0	8040
16	**S5**	2.50	1	292	68	174	132	15500
17	**S5**	2.50	0.2	292	68	913	21.4	11300
18	**S6**	2.50	0.2	292	68	860	21.4	12300
19	**S7**	2.50	0.2	292	68	870	9.3	5420
20	**S11**	2.60	0.2	292	68	954	28.9	18000
21	**S5**	2.50	0.2	292	17	185	29.8	3740
22	**S5**	2.50	0.2	292	34	364	29.3	7430
23	**S5**	2.50	0.2	292	136	1644	15.7	18300
24	**S5**	1.25 [h]	0.2	292	68	441	7.8	2890
25	**S5**	1.88 [h]	0.2	292	68	388	16.6	4630
26	**S5**	2.50 [h]	0.2	292	68	420	19.8	5370
27	**S5**	3.13 [h]	0.2	292	68	409	16.1	4590
28	**S5**	2.50	0.2	282	68	1010	27.9	1850
29	**S5**	2.50	0.2	302	68	774	15.8	8000
30	**S5**	2.50	0.25 [i]	292	68	714	24.5	11600
31	**S5**	2.50	0.31 [j]	292	68	640	62.0	27100

Standard condition: $[C_2C_1Im][FAP]$, $\alpha_{IL} = 0.3$; $\dot{V}_{ethene}$ = 5.1 Nml min⁻¹, $\tau \approx 1.3$ s. a) Nickel loading related to support; b) total mass of catalyst in reactor; c) time to reach 50 % initial conversion; d) fixed bed, feed not purified; e) fluidized bed, feed not purified; g) fixed bed, feed purified; h) other charge of nickel precursor; i) $\alpha_{IL} = 0.6$; j) $\alpha_{IL} = 0.9$.

Although the use of purified ethene feed gas in combination with a fluidized bed instead of a fixed bed improved the activity and stability of the Ni-SILP catalyst; however, the deactivation process could not be suppressed completely. We therefore investigated the effect of different support materials on the deactivation behavior of the SILP catalyst in fluidized bed operation.

Support material variation

In this set of experiments we focused on the supports exhibiting a good fluidization behavior, namely **S5**, **S6** and **S11** and the Geldart B support **S7** as a reference support material (Entries 17-20, Table 2). Figure 6 compiles the obtained TOF and TON over TOS data for the different SILP catalysts with constant metal content of Ni at $w_{Ni} = 2.50$ mg$_{Ni}$ g$_{support}^{-1}$.
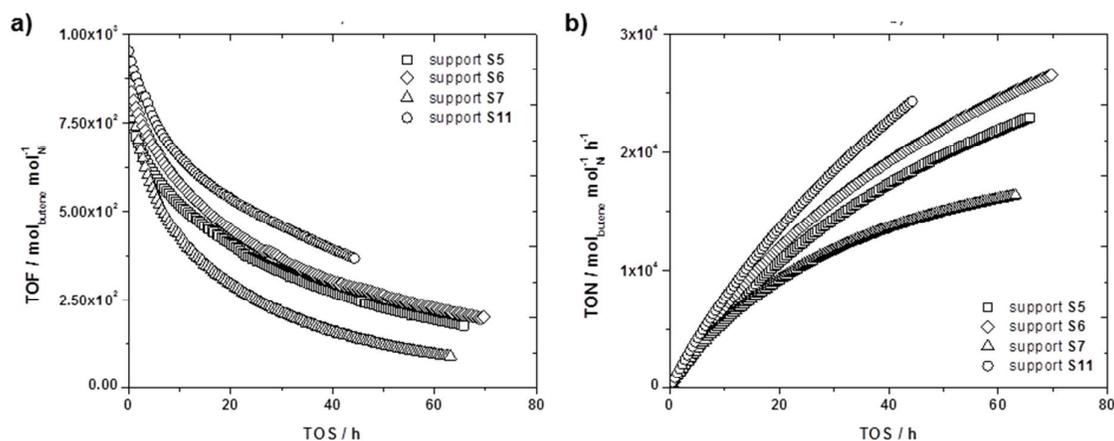
Figure 6. TOF and TON over TOS of the ethene dimerization with SILP catalyst ([(mall)Ni-dppanis][SbF₆] 1, w_{Ni} = 2.50 mg_{Ni} $g_{support}^{-1}$, [C₂C₁Im][FAP], α_{IL} = 0.3) with different support materials S5, S6, S7 and S11 in a fluidized bed reactor; m_{SILP} = 200 mg, $T_{reactor}$ = 292 K, p_{ethene} = 68 mbar, V_{ethene} = 5.1 Nml min⁻¹, $\tau \approx$ 0.3 s, $p_{reaction}$ = 1 bar.

The **S7** based SILP catalyst (Entry 19) formed a bubbling fluidized bed at the given flow parameters, consequently the SILP catalyst based on the latter showed the poorest stability and thus the lowest $TON_{t1/2}$ of 5420 mol_{butene} mol_{Ni}^{-1} and the lowest TON after 40 h of 13800 (due to locally high ethene concentration and thus – presumably – to higher temperatures. Both SILP catalysts with almost identical support **S5** and **S6** showed approximately the same catalytic performance (Entry 17 and 18) with slight advantages in activity and stability for the latter. The **S11** based SILP catalysts (Entry 20) showed the slowest deactivation with a half-life time of nearly 29 h and also the highest TOF of 954 mol_{butene} mol_{Ni}^{-1} h^{-1}. As a consequence, this catalyst gave the highest $TON_{t1/2}$ of 18000 mol_{butene} mol_{Ni}^{-1} and a final TON after 40 h of almost 25000 mol_{butene} mol_{Ni}^{-1}. Although the TOF of the **S11** based SILP exceeded the TOF found for **S5**, **S6** and **S7**, the effective reaction rate related to the catalytic volume of the **S11** based catalyst was around 1.5 to 2 times lower than the reaction rates for the other supports. This specific difference probably resulted from the differing inner surface, pore volume, and pore diameter of the supports **S11**, **S5/S6,** and **S7** (see Table 1). As a result of the smaller inner surface and the different pore volume, the thickness of the IL film inside the pores was increased. With a constant pore filling degree the theoretical film thickness was one order of magnitude higher using **S11** (7.64 nm) compared to **S5** (0.72 nm). Additionally, the calculated concentration of Ni-precursor dissolved in the dispersed IL was varied in order to keep ω_{Ni} constant. For **S11** based SILP catalysts 102 mol m_{IL}^{-3} were used, while for **S5** systems 198 mol m_{IL}^{-3} were required. Regarding the achievable TON values for the different catalysts it seemed to be advantageous to have Geldart A porous supports with a high pore volume and lower inner surface, since the effective reaction rate related to the catalytic volume was decreased. Obviously, the smaller reaction heat released can then be more effectively distributed throughout the catalyst bed. Regarding this aspect increasing the pore filling should result in a similar effect on the deactivation process.

Variation of pore filling degree

Entries 17, 30, and 31 in Table 2 summarize the ethene dimerization performance of Ni-SILP catalysts with different pore fillings of α_{IL} = 0.3, 0.6 and 0.9. In these investigations the TOF of the catalysts as well as the volume specific reaction rate were reduced as a consequence of the increase in pore filling of the SILP catalysts. The catalyst with a pore filling of α_{IL} = 0.3 (Entry 17) showed the highest activity with a TOF_{max} of 913 mol_{butene} mol_{Ni}^{-1} h^{-1}, that was lowered for α_{IL} = 0.6 (Entry 30) to a

TOF$_{max}$ of 714 mol$_{butene}$ mol$_{Ni}^{-1}$ h^{-1} and for α_{IL} = 0.9 (Entry 31) to a TOF$_{max}$ of 640 mol$_{butene}$ mol$_{Ni}^{-1}$ h^{-1}. Since the Ni loading was kept constant at w$_{Ni}$ = 2.50 mg$_{Ni}$ g$_{support}^{-1}$, this trend reflects the lower nickel concentration in the ionic liquid film and the influence of mass transport limitations, in particular limitations due to the increasing thickness of the relatively viscous ionic liquid film. In fact, the effective reaction rate is reduced by the decrease of the mass transfer area inside the SILP catalyst pellet and by the longer diffusional path lengths of the substrate in the thicker ionic liquid film. The BET surface area of the particular SILP catalysts is linearly lowered due to an increase of pore filling. Interestingly, this lower activity of the nickel catalyst in the ionic liquid film resulted in an improved stability of the SILP material, since the lower rate was naturally accompanied with less heat generation. Also, the thicker film could distribute the reaction heat much better in the liquid phase; thereby, stabilizing the temperature sensitive nickel complex. Using the SILP material with the thickest ionic liquid film, a total TON of 27100 was obtained, which clearly demonstrates the improved stability.

Variation of nickel loading

To test the influence of mass transport limitation, we varied the specific amount of the complex Ni-dppanis related to the neat support material from 0.125 wt.-% to 0.313wt.-% (Entry 24-27). Thereby the concentration of Ni inside the IL film was altered from 99.35 mol m$_{IL}^{-3}$ to 248.37 mol m$_{IL}^{-3}$. Figure 7 displays the volume specific effective reaction rate over TOS as well as the dependency of the initial effective reaction rate from the catalyst complex concentration of the four named experiments.
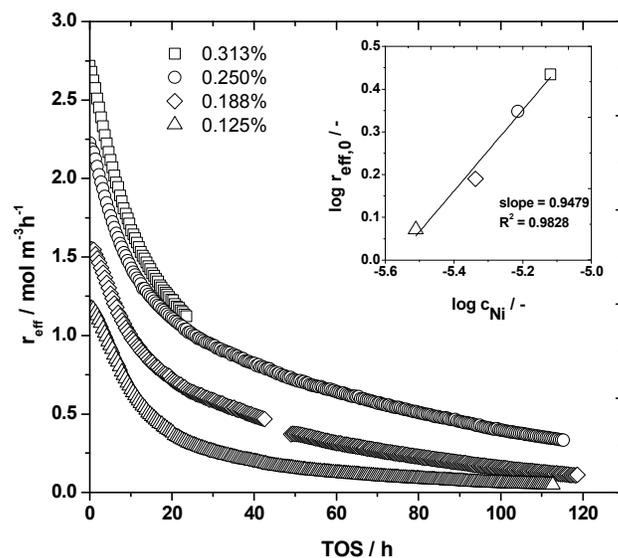
Figure 7. Effective reaction rate over TOS of SILP catalysts comprising [(mall)Ni-dppanis][SbF$_6$] 1, [C$_2$C$_1$Im][FAP], S5, α_{IL} = 0.3 with different Ni-loadings w$_{Ni}$ = 1.25, 1.88, 2.50 and 3.13 mg$_{Ni}$ g$_{support}^{-1}$ in a fluidized bed reactor; m$_{cat}$ = 200 mg, V$_{ethene}$ = 5.1 Nml min^{-1}, $\tau \approx 0.3$ s, T = 292 K, p$_{reaction}$ = 1 bar.

While the maximum TOF values of these experiments stayed in the same range of 388 to 441 mol$_{butene}$ mol$_{Ni}^{-1}$, the effective reaction rate increased with increasing amount of Ni precursor. The reaction order regarding Ni could be determined as a nearly first order reaction, indicating the absence of mass transport influence at this low ionic liquid loading. The longest half life time, and thus also the highest TON$_{t1/2}$ was identified for the catalyst with a Ni loading of w$_{Ni}$ = 0.250 wt.-%. Based on the

assumption of lower reaction rates of diluted systems resulting in higher stability, this effect was probably counterbalanced by oxygen and water impurities still present in the purified feed gas, leading to faster deactivation of the lower concentrated nickel.

Variation of ethene partial pressure

Applying the standard SILP catalyst at 292 K, the partial pressure of ethene was varied by adjusting the volume flow of ethene while keeping the total volume flow and residence time constant. Figure 8 depicts the measured TOF over TOS for four different partial pressures of ethene ranging from 17 mbar to 136 mbar and the resulting reaction order of ethene calculated from the initial effective reaction rate and the corresponding deactivation parameter $k_{d,2}$ (Entries 17 and 21-23).
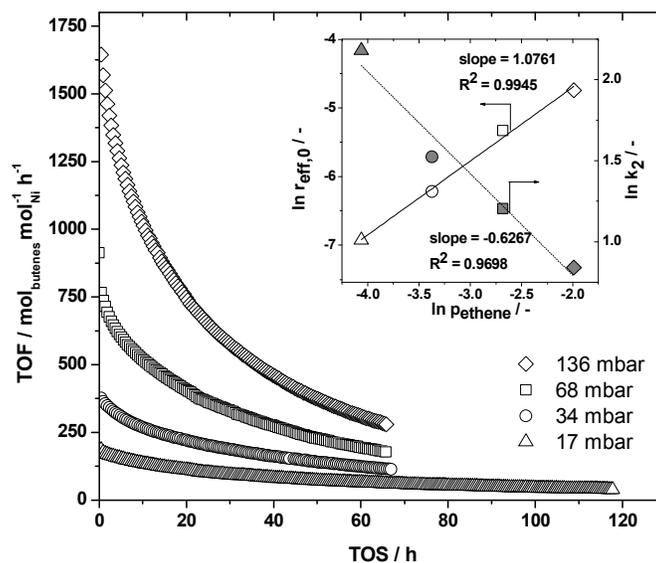
Figure 8. *Turn over frequency over time on stream of the standard SILP catalyst at different partial pressure of ethene in a fluidized bed reactor - determination of the reaction order of ethene by linearization of initial effective reaction rate and dependency of deactivation coefficient $k_{d,2}$ on the ethene pressure; [(mall)Ni-dppanis][SbF$_6$]* **1**, *w_{Ni} = 2.50 mg$_{Ni}$ g$_{support}$$^{-1}$, [C$_2C_1$Im][FAP]*, **S5**, *$\alpha_{IL}$ = 0.3; m_{cat} = 200 mg, V_{ethene} = 1.28 – 10.2 Nml min^{-1}, $\tau \approx 0.3$ s, T = 292 K, $p_{reaction}$ = 1 bar.*

The differential analysis of $\ln(r_{eff})$ vs. $\ln(p_{ethene})$ (see insert) indicates a first order reaction of ethene. We additionally noticed an influence of the partial pressure on the deactivation, exemplified by the deactivation parameter $k_{d,2}$ (for details see next chapter). Surprisingly, the deactivation seemed to be decelerated with increasing partial pressure of ethene, since $k_{d,2}$ decreased while TON$_{t1/2}$ increased. This observation is in conflict with the assumption that a slower reaction rate would result in a reduction of the released reaction heat and would therefore result in an improved stability of the Ni-SILP catalyst. We interpret this result as a hint for an additional deactivation mechanism of the cationic Ni-dppanis complex apart from thermal decomposition and poisoning by gas impurities. Our observation would be in line with the assumption of a deactivation route involving the reaction of two active Ni complexes with one another in case insufficient ethene is present.[35] This aspect will be developed in more detail below.

Deactivation kinetics and modeling

The deactivation behavior of cationic Ni SILP-type catalysts based on the support **S5** were studied in more detail under fluidized bed operation in a diluted ethene stream in the range of 282 to 302 K. The applied temperature range was restricted by the temperature sensitivity of the catalyst and by the agglomeration of SILP catalyst particles as a consequence of oligomer condensation in the catalytic fluidized bed at very low temperatures. For a first order reaction in ethene and Ni-complex, the time dependent effective reaction rate can be described with Equation (1).

$$r_{eff}(t) = k'_{eff} \cdot c_{Ni}(t) \qquad \text{with } k'_{eff} = k_{eff} \cdot c_{ethene} \tag{1}$$

For a first order deactivation mechanism, the amount of Ni is reduced within the reaction time t according to Equation (2). The effective reaction rate drops accordingly (Equation (3)).

$$c_{Ni}(t) = c_{Ni,0} \cdot e^{-k_{d,1}t} \tag{2}$$

$$r_{eff}(t) = r_0 \cdot e^{-k_{d,1}t} \tag{3}$$

Alternatively, a second order deactivation mechanism can be considered, leading to the effective reaction rate represented by Equations (4) and (5), respectively.

$$\frac{1}{c_{Ni}(t)} = \frac{1}{c_{Ni,0}} + k_{d,2}t \tag{4}$$

$$\frac{1}{r_{eff}(t)} = \frac{1}{r_{eff,0}} + k_{d,2}t \tag{5}$$

Figure 9 displays the experimental dimerization result in form of Equations (3) and (5). The graphs have been obtained by plotting the logarithmic r_{eff} and r_{eff}^{-1} versus TOS. The slope of the three experiments with different temperatures represents the deactivation constant $k_{d,1}$ (ln r_{eff} over TOS) for a first order and $k_{d,2}$ (r_{eff}^{-1} over TOS) for a second order deactivation.

Figure 9. *Determination of the deactivation coefficient $k_{d,1}$ for the assumption of a first order and $k_{d,2}$ for the assumption of a second order catalyst deactivation process at the three*

*different temperatures 282, 292 and 302 K and determination of the activation energy of deactivation; SILP catalysts with Ni-dppanis[(mall)Ni-dppanis][SbF$_6$] **1** complex, w_{Ni} = 2.50 g_{Ni} $g_{support}^{-1}$, **S5**, [C$_2$C$_1$Im][FAP], a_{IL} = 0.3; m_{SILP} = 200 mg, p_{ethene} = 68 mbar, V_{ethene} = 5.1 Nml min^{-1}, $t \approx 0.3$ s, $p_{reaction}$ = 1 bar.*

While the plot of the logarithmic r_{eff} deviates strongly from linearization, r_{eff}^{-1} matches with a coefficient of determination of R^2 > 0.994 the linear behavior required by the deactivation model indicates a second order deactivation process. With the deactivation constants $k_{d,2}$ at four different temperatures (one additional experiment at 272 K is shown in the Supporting Information), an activation energy of deactivation $E_{A,d}$ of 23.2 kJ mol^{-1} can be determined. A consequence of this relatively low value is that it is not possible to suppress catalyst deactivation completely by applying low temperatures.

A dimensionless reaction process for the observed second order catalyst deactivation is given by transformation of Equation (5) into Equation (6).

$$\frac{r_{eff}(t)}{r_{eff,0}} = \frac{1}{1 + r_{eff,0} \cdot k_{d,2} \cdot t} \tag{6}$$

With the known initial reaction rate and rate constant of deactivation the course of the reaction can be predicted. As the deactivation coefficient is not only temperature dependent but also influenced by the partial pressure of ethene, the deactivation coefficient $k_{d,2}$ has to be described as a function of both. In the Supporting Information we give values for $k_{d,2}$ (in l mol^{-1}) as a function of the reaction temperature and the partial pressure of ethene. In Figure 10 the mathematical modeling of the deactivation process is compared with the measured course of the reaction for the three temperatures 282, 292, and 302 K. The lines reflect the calculated deactivation process for the temperatures between 252 and 312 K in steps of 10 K, assuming an almost unchanged initial reaction rate, as we surprisingly found for the temperatures between 282 and 302 K.

*Figure 10. Comparison of the mathematical modelling of the catalyst deactivation process with experimental results – the applied model includes a second order deactivation process and a $E_{A,d}$ value of 23.2 kJ mol^{-1} - SILP catalysts comprising [(mall)Ni-dppanis][SbF$_6$] **1**,*

$w_{Ni} = 2.50 \ mg_{Ni} \ g_{support}^{-1}$, S5, [$C_2C_1Im$][FAP], $a_{IL} = 0.3$; $m_{SILP} = 200 \ mg$, $p_{ethene} = 68 \ mbar$, $V_{ethene} = 5.1 \ Nml \ min^{-1}$, $t \approx 0.3 \ s$, $p_{reaction} = 1 \ bar$.

The mathematical modeling of the deactivation process fits very well for an assumed second order deactivation process. For comparison, the mismatching fit for an assumed first order deactivation process can be seen in SI. These results illustrate that even for a temperature as low as 252 K the deactivation process of the catalyst would be still significant if the same deactivation mechanism prevails at this low temperature. However, at such low temperatures, condensation of oligomerization products in the SILP catalyst would cause major problems.

Conclusion

In this study, we adapted cationic Nickel based SILP catalysts in a fluidized bed reaction for the first time. We therefore characterized different SiO_2-based porous support materials with regard to their fluidization behavior and monitored the influence of IL loading of the support on the fluidization characteristics. By adding an IL to the support, the minimum fluidization velocity was increased (for pore filling $\alpha_{IL} = 0.9$ of around 27 %) and the overall pressure drop became more pronounced. However, even with a high pore filling of up to 90 % fluidization was still possible. We could not observe a major drawback like agglomeration of the SILP catalysts as a result of the IL impregnation. Our catalytic experiments establish that a dilution with inert gas was required for the dimerization of ethene with cationic Ni SILP-type catalysts in a fluidized bed operation, since a process with pure ethene led to an immediate deactivation by the released reaction heat and an agglomeration of SILP catalysts due to condensation of higher boiling products. The comparison of a fixed bed and fluidized bed process indicated that the improved distribution of the released reaction heat in the latter was advantageous for the stability of the cationic Ni SILP-type catalysts. The investigation of the influence of support materials, pore filling, and reaction temperature on the deactivation behavior of the SILP catalysts showed that higher pore filling degrees gave lower reaction rates and, in consequence, generated less reaction heat. For temperature sensitive Nickel catalysts this lower heat generation resulted in prolonged stability. Additionally, an improved removal or distribution of the reaction heat by higher heat conductivity and thicker ionic liquid films proved advantageous for the reaction.

The variation of the partial pressure of ethene showed opposing trends. With increasing partial pressure the rate of reaction increased, while at the same time deactivation was reduced. We attributed this to a deactivation mechanism of Ni complexes reacting with themselves or impurities when the availability of ethene is low while too high ethene concentrations would result in high reaction rate, thus generating too much heat inside the SILP catalyst pellets.

Applying SILP catalysts in the fluidized bed reactor with its good isothermicity, we were also able to determine the deactivation kinetics of the ethene dimerization with cationic Ni based SILP catalysts in diluted feed. The activation energy of deactivation for the particular SILP material comprising the Ni-dppanis precursor dissolved in [C_2C_1Im][FAP] ($\alpha_{IL} = 0.3$ on the support **S5**) was determined to be $E_{A,d} = 23.2 \ kJ \ mol^{-1}$. The results indicate that even at temperatures as low as 252 K catalyst deactivation would still be observed if the same catalyst deactivation mechanism prevails. At this temperature, however, product condensation would be a major practical issue. Future work will focus on the development of cationic Ni complexes with higher robustness against temperature and low ethylene pressures. Catalytic oligomerization using SILP catalysts in a fluidized bed reactor has in principal proven to be an interesting and feasible concept.

Acknowledgements

Experimental

All air- and moisture-sensitive experiments and syntheses were carried out in an inert glovebox or under argon atmosphere using standard Schlenk techniques. 1-ethyl-3-methylimidazolium tris(pentafluoroethyl)trifluorophosphate $[C_2C_1Im][eFAP]$ (purity $\geq$ 99.0 %, water content $\leq$ 100 ppm, halide content $\leq$ 100 ppm) and 1-ethyl-3-methylimidazolium tetrafluoroborate $[C_2C_1Im][BF_4]$ were purchased from Merck KGaA and used without further purification. The Ni catalyst complex $[(mall)Ni\text{-}dppanis][SbF_6]$ (dppanis = (2-methoxyphenyl)diphenylphosphine) that was applied in the dimerization of ethene was synthesized by Dr. Nicola Taccardi, Chemical Reaction Engineering, FAu Erlangen-Nürnberg, according to literature known preparation routes. The support materials Carrier 1-4 (**S1-S4**), Spherical A (**S5**) and B (**S6**) was provided by Clariant. The support materials silica 100 (**S7**) and silica gel 60 (**S8**) and PharmPrep 60 cc (**S12**) was purchased from Merck. Trisoperl 1200 45-65 µm (**S9**) and 20-35 µm (**S11**) and Trisoperl 500 (80-130 µm) (**S10**) was purchased from VitraBio™. Each of the support materials were calcined prior to application by following procedure: The support material was heated up from room temperature to 423 K with a heating rate of 4 K min^{-1}. In order to remove water out from the pores the temperature of 423 K was kept constant for two hours. Afterwards, the support was heated up to 873 K with a heating rate of 4 K min^{-1}. Before the material finally cooled down to room temperature, the temperature of 873 K was maintained for another 12 h. The pretreated material was evacuated overnight and eventually stored in an inert gas box.
The SILP catalysts were prepared by dissolution of the self-activating Ni-methallyl complex and the required amount of ionic liquid in dichloromethane (< 0,004% H$_2$O stabilized with 50.00 ppm 2-methyl-2-buten). After addition of the desired amount of the support material the solvent of the suspension was removed within 30 min at 273 K. The catalyst was cooled for transportation at 273 K and stored in the glovebox at 253 K. The formal pore filling α_{IL} of the SILP catalyst was calculated according to Equation (7).

$$\alpha_{IL} = \frac{V_{IL}}{m_{support} \cdot V_{pore}} \quad \left[\frac{cm_{IL}^3 \cdot g_{support}}{g_{support} \cdot cm_{pore}^3} \right] \tag{7}$$

The content of Ni of the SILP catalysts was calculated according to Equation (8).

$$\omega_{Ni} = \frac{m_{Ni}}{m_{support}} = \frac{m_{Ni\text{-}precursor} \cdot M_{Ni}}{m_{support} \cdot M_{Ni\text{-}precursor}} \quad \left[\frac{mg_{Ni}}{g_{support}} \right] \tag{8}$$

In order to investigate the effect of various IL loadings on the stability of the SILP catalyst, samples with pore fillings of $\alpha_{IL} = 0.3$, 0.6 and 0.9 were prepared. The specific pore volume and the specific BET surface area of the original support materials were determined using a Quantrachrome Quadrasorb SI Micrometrics ASAP instrument. The particle size distribution was measured at the chair of particle technology, University of Erlangen-Nuremberg with a Malvern Mastersizer 2000.

Pressure drop curves were recorded with a GDH precision digital manometer for pressure range of 0-199.9 mbar. These experiments were conducted in a glass reactor with an inner diameter of 15 mm. The nitrogen flow was adjusted with a mass flow controller in the range of 1-50 ml min^{-1}.

All catalytic experiments were conducted within continuous gas phase reactor built in-house. A schematic view of the dimerization set-up is depicted in Figure 11.
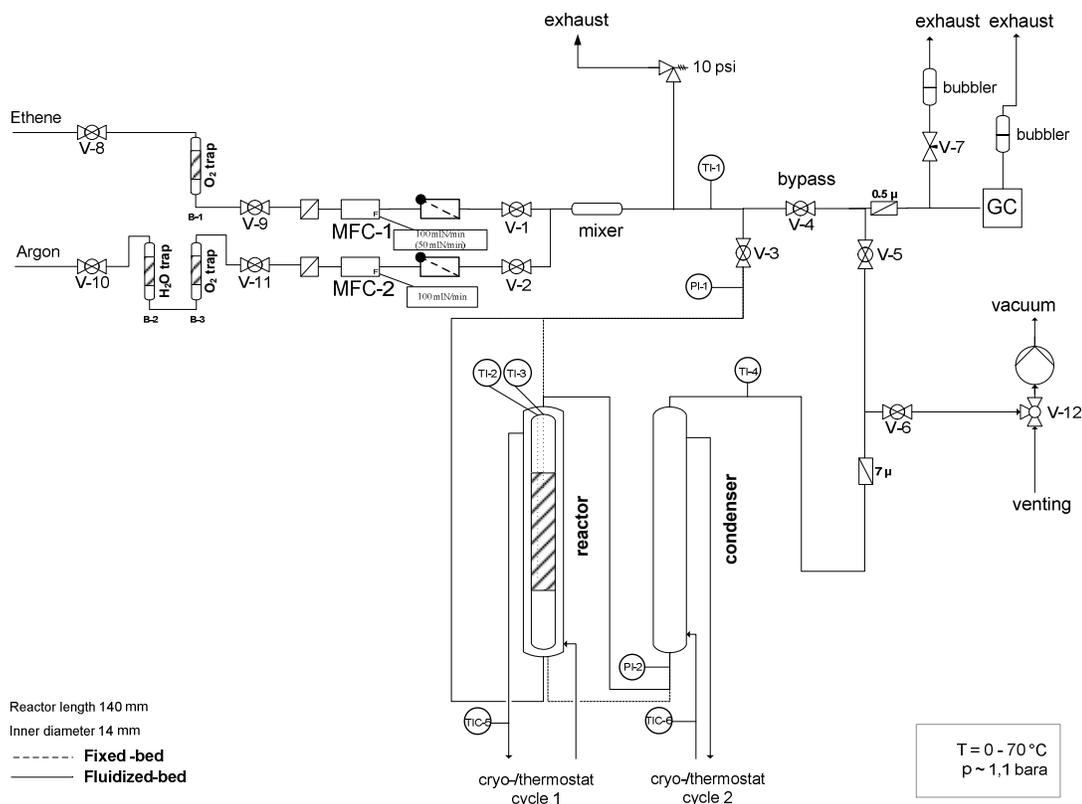
Figure 11. *Schematic view of the experimental set up for the gas phase dimerization of ethene in a fluidized bed or fixed bed reactor.*

The gas phase experiments were carried out with ethene (3.5, ≥ 99.95 %, Linde Gas AG) as substrate for the dimerization and argon (4.8, ≥ 99.998 %, Linde Gas AG) as inert carrier gas. For additional purification, the ethene feed was cleaned with a high-capacity oxygen trap (Restek) to remove oxygen to less than 15 ppb. We refer to this ethene quality as "purified ethene". Argon was purified with a high-capacity moisture trap (Restek, water content ≤ 15 ppb) and an aforementioned high-capacity oxygen trap (all experiments except *entry 17* and *18*). Each gas was dosed via a multi range mass flow controller (Bronkhorst). The adjustable volume flow is ranging from 1-50, 1-100 and 1-150 ml min^{-1}. Both gases were mixed in a static mixer and subsequently passed through the double-walled glass reactor either upstream or downstream. Due to flexible connections at the reactor in- and outlet, both operation modes (fixed bed and fluidized bed) could be realized. For reaching steady-state conditions the reactor was by-passed. After passing through the reactor the gas stream was analyzed online with a gas chromatograph (Agilent 7820A GC).

In preparation of the dimerization the reactor was evacuated over several hours at 343 K and $1·10^{-2}$ mbar. Afterwards the pressure was adjusted with argon at 292 K. At the beginning of the reaction the cooled SILP-catalyst was filled in the reactor under argon stream (V = 10 ml min^{-1}). In addition the reactor was subsequently purged with argon (V = 100 ml min^{-1}) in order to avoid moisture and oxygen

contaminants for 2 min and closed afterwards with a slight over pressure of 200 mbar. Before the reaction started the volume flows of ethene and argon were adjusted over the bypass. Reaching continuous flow conditions the bypass was closed and the reactor valves were opened. With the reaction the online measurement was started simultaneously.

References

[1] *Evolving Propylene Sources, Solution to Supply Shortages?* Chemsystems Prospectus, January **2012**.

[2] H. Zimmermann, R. Walzl, *Ethylene* in *Ullmann's Encyclopedia of Industrial Chemistry*, Wiley-VCH Verlag GmbH & Co. KGaA, **2000**.

[3] P. Eisele, R. Killpack, *Propene* in *Ullmann's Encyclopedia of Industrial Chemistry*, Wiley-VCH Verlag GmbH & Co. KGaA, **2000**.

[4] a) H. Oikawa, Y. Shibata, K. Inazu, Y. Iwase, K. Murai, S. Hyodo, G. Kobayashi, T. Baba, *Appl. Catal. A: Chem*. **2006**, *312*, 181-185; b) T. Baba, H. Sawada, *Phys. Chem. Chem. Phys*. **2002**, *4*, 3919-3923.

[5] B. Lin, Q. Zhang, Y. Wang, *Ind. Eng. Chem. Res*. **2009**, *48*, 10788-10795.

[6] P.P. O'Neill, J.J. Rooney, *J. Am. Chem. Soc*. **1972**, *94*, 4383-4384.

[7] J. Engelhardt, *J. Catal*. **1980**, *62*, 243-252.

[8] T. Yamaguchi, Y. Tanaka, K. Tanabe, *J. Catal*. **1980**, *65*, 442-447.

[9] M. Taoufik, E. Le Roux, J. Thivolle-Cazat, J.-M. Basset, *Angew. Chem. Int. Ed*. **2007**, *46*, 7202-7205.

[10] a) M. Iwamoto, Y. Kosugi, *J. Phys. Chem. C* **2006**, *111*, 13-15; b) K. Ikeda, Y. Kawamura, T. Yamamoto, M. Iwamoto, *Catal. Commun*. **2008**, *9*, 106-110; c) M. Iwamoto, *Molecules* **2011**, *16*, 7522-7550.

[11] T. Lehmann, T. Wolff, V.M. Zahn, P. Veit, C. Hamel, A. Seidel-Morgenstern, *Catal Commun*. **2011**, *12*, 368-374.

[12] J. Scholz, V. Hager, X. Wang, F.T.U. Kohler, M. Sternberg, M. Haumann, N. Szesni, K. Meyer, P. Wasserscheid, *ChemCatChem*, **2013**, DOI: 10.1002/cctc.201300636.

[13] I. Brassat, W. Keim, S. Killat, M. Möthrath, P. Mastrorilli, C.F. Nobile, G.P. Suranna, *J. Mol. Catal. A: Chem*. **2000**, *157*, 41-58.

[14] F. Speiser, P. Braunstein, L. Saussine, *Acc. Chem. Res*. **2005**, *38*, 784-793.

[15] U. Müller, W. Keim, C. Krüger, P. Betz, *Angew. Chem. Int. Ed*. **1989**, *28*, 1011-1013.

[16] G. Wilke, *Angew. Chem. Int. Ed*. **1988**, *27*, 185-206.

[17] P.J. Flory, *J. Am. Chem. Soc*. **1940**, *62*, 1561-1565.

[18] R.B.A. Pardy, I. Tkatchenko, *J. Chem. Soc., Chem. Commun*. **1981**, 49-50.

[19] a) D. Matt, M. Huhn, J. Fischer, A. De Cian, W. Kläui, I. Tkatchenko, M.C. Bonnet, *J. Chem. Soc., Dalton Trans*. **1993**, 1173; b) P. Kuhn, D. Sémeril, C. Jeunesse, D. Matt, P. Lutz, R. Welter, *Eur. J. Inorg. Chem*. **2005**, 1477-1481; c) P. Kuhn, D. Sémeril, C. Jeunesse, D. Matt, M. Neuburger, A. Mota, *Chem. Eur. J*. **2006**, *12*, 5210-5219.

[20] a) K. Hirose, W. Keim, *J. Mol. Catal*. **1992**, *73*, 271-276; b) W. Keim, R.P. Schulz, *J. Mol. Catal*. **1994**, *92*, 21-33; c) J. Heinicke, M. He, A. Dal, H.-F. Klein, O. Hetche, W. Keim, U. Flörke, H.-J. Haupt, *Eur. J. Inorg. Chem*. **2000**, 431-440; d) J. Heinicke, M. Köhler, N. Peulecke, W. Keim, *J. Catal*. **2004**, *225*, 16-23.

[21] a) J. Pietsch, P. Braunstein, Y. Chauvin, *New J. Chem*. **1998**, *22*, 467-472; b) P. Braunstein, Y. Chauvin, S. Mercier, L. Saussine, *C. R. Chimie*, **2005**, *8*, 31-3.

[22] Z.J.A. Komon, X. Bu, G.C. Bazan, *J. Am. Chem. Soc*. **2000**, *122*, 1830-1831.

[23] J.M. Malinoski, M. Brookhart, *Organometallics*, **2003**, *22*, 5324-5335.

[24] I. Brassat, W. Keim, S. Killat, M. Möthrath, P. Mastrorilli, C.F. Nobile, G.P. Suranna, *J. Mol. Catal. A: Chem*. **2000**, *157*, 41-58.

[25] M.C. Bonnet, F. Dahan, A. Ecke, W. Keim, R.P. Schulz, I. Tkatchenko, *J. Chem. Soc., Chem. Commun*. **1994**, 615-616.

[26] R.F. de Souza, K. Bernardo-Gusmão, G.A. Cunha, C. Loup, F. Leca, R. Réau, *J. Catal*. **2004**, *226*, 235-239.

[27] a) Y. Chauvin, B. Gilbert, I. Guibard, *J. Chem. Soc., Chem. Commun*. **1990**, 1715-1716; b) Y. Chauvin, S. Einloft, H. Olivier, *Ind. Eng. Chem. Res*. **1995**, *34*, 1149-1155; c) Y. Chauvin, H. Olivier, C.N. Wyrvalski, L.C. Simon, R.F. de Souza, *J. Catal*. **1997**, *165*, 275-278.

[28] H. Olivier, P. Laurent-Gérot, *J. Mol. Catal. A: Chem*. **1999**, *148*, 43-48.

[29] a) L.C. Simon, J. Dupont, R.F. de Souza, *Appl. Catal. A: General* **1998**, *175*, 215-220; b) K. Bernardo-Gusmão, L.F. Trevisian Queiroz, R.F. de Souza, F. Leca, C. Loup, R. Réau, *J. Catal*. **2003**, *219*, 59-62.

[30] B. Ellis, W. Keim, P. Wasserscheid, *Chem. Commun*. **1999**, 337-338.

[31] a) C.P. Mehnert, R.A. Cook, N.C. Dispenziere, M. Afeworki, *J. Am. Chem. Soc*. **2002**, *124*, 12932-12933; b) C.P. Mehnert, E.J. Mozeleski, R.A. Cook, *Chem. Commun*. **2002**, 3010-3011.

[32] A. Riisager, R. Fehrmann, S. Flicker, R. van Hal, M. Haumann, P. Wasserscheid, *Angew. Chem. Int. Ed*. **2005**, *44*, 815-819.

[33] For recent reviews see: a) Y. Gu, G. Li, *Adv. Synth. Catal*. **2009**, *351*, 817-847; b) C. Van Doorslaer, J. Wahlen, P. Mertens, K. Binnemans, D. De Vos, *Dalton Trans*. **2010**, *39*, 8377-8390; c) J. Scholz, M. Haumann, *Supported Ionic Liquid Thin Film Technology* in *Nanomaterials in Catalysis* (Eds.: P. Serp, K. Philippot), Wiley-VCH Verlag GmbH & Co. KGaA, **2013**.

[34] a) F. Kohler, D. Roth, E. Kuhlmann, P. Wasserscheid, M. Haumann, *Green Chem*. **2010**, *12*, 979-984; b) S. Werner, N. Szesni, M. Kaiser, R.W. Fischer, M. Haumann, P. Wasserscheid, *ChemCatChem* **2010**, *2*, 1399-1402; c) M. Jakuttis, A. Schönweiz, S. Werner, R. Franke, K.-D. Wiese, M. Haumann, P. Wasserscheid, *Angew. Chem. Int. Ed*. **2011**, *50*, 4492-4495.

[35] A. Berkefeld, S. Mecking, *J. Am. Chem. Soc*. **2009**, *131*, 1565-1574.

[36] K. Noda, S. Uchida, T. Makino, H. Kamo, *Powder Technology* **1986**, 46(2-3), 149-54.

[37] S. K. Gupta, V. K. Agarwal, S. N. Singh, V. Seshadri, David Mills, J. Singh, Chandra Prakash, *Powder Technology* **2009**, 196(3), 263-271.

[38] D. Geldart, *Powder Technology* **1973**, 7(5), 285-292.

Table of contents

Dimerization of ethene in a fluidized bed reactor using Ni-based Supported Ionic Liquid Phase (SILP) catalysts

Florian T. U. Kohler [a], Konstantin Gärtner [a], Veit Hager [a], Marco Haumann [a], Michelle Sternberg [b], Xinjiao Wang [b], Normen Szesni [c], Karsten Meyer [b], Peter Wasserscheid [a]*

[a] Department of Chemical and Bioengineering, Reaction Engineering, University Erlangen-Nuremberg, Egerlandstraße 3, D-91058 Erlangen, Germany; e-mail: peter.wasserscheid@crt.cbi.uni-erlangen.de
[b] Department of Chemistry and Pharmacy, Inorganic Chemistry, University Erlangen-Nuremberg, Egerlandstraße 1, D-91058 Erlangen, Germany
[c] Clariant Produkte (Deutschland) GmbH, Waldheimer Straße 13, 83052 Bruckmühl, Germany
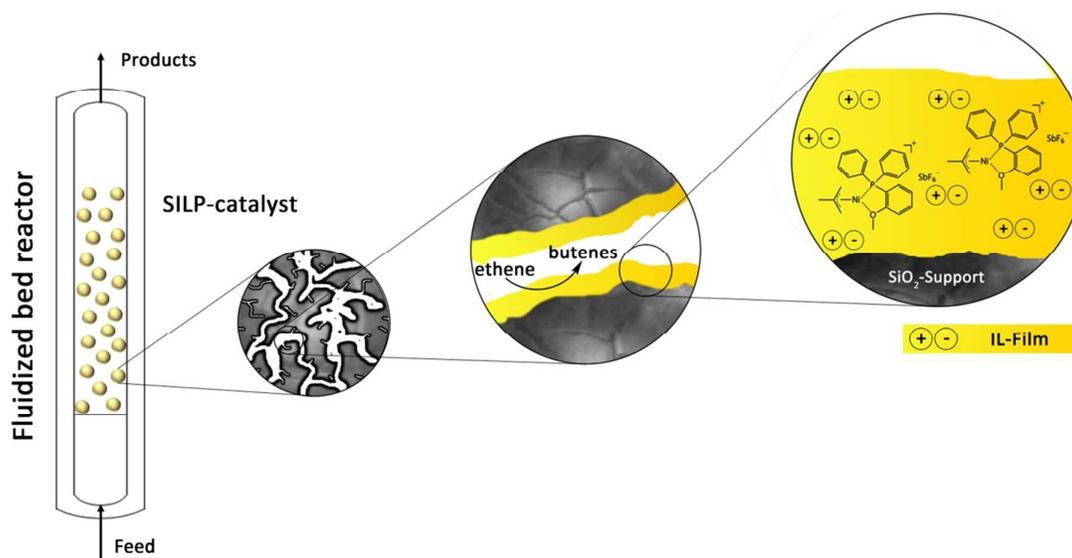
Ethene dimerization to 2-butenes was catalyzed by Ni-SILP complexes for the first time in a fluidized bed to improve heat removal.